



Original article

Novel small molecule inhibitors targeting the “switch region” of bacterial RNAP: Structure-based optimization of a virtual screening hit



J. Henning Sahner, Matthias Groh, Matthias Negri, Jörg Haupenthal, Rolf W. Hartmann*

Pharmaceutical and Medicinal Chemistry, Saarland University & Helmholtz Institute for Pharmaceutical Research Saarland (HIPS), Department of Drug Design and Optimization, Campus C2 3, 66123 Saarbrücken, Germany

ARTICLE INFO

Article history:

Received 4 April 2013

Received in revised form

26 April 2013

Accepted 27 April 2013

Available online 7 May 2013

Keywords:

Bacterial RNAP inhibitor

Switch region

Myxopyronin

Ureidothiophene carboxylic acid

QSAR

Antibacterial agent

ABSTRACT

Rising resistance against current antibiotics necessitates the development of antibacterial agents with alternative targets. The “switch region” of RNA polymerase (RNAP), addressed by the myxopyronins, could be such a novel target site. Based on a hit candidate discovered by virtual screening, a small library of 5-phenyl-3-ureidothiophene-2-carboxylic acids was synthesized resulting in compounds with increased RNAP inhibition. Hansch analysis revealed π (lipophilicity constant) and σ (Hammett substituent constant) of the substituents at the 5-phenyl moiety to be crucial for activity. The binding mode was proven by the targeted introduction of a moiety mimicking the enecarbamate side chain of myxopyronin into the hit compound, accompanied by enhanced RNAP inhibitory potency. The new compounds displayed good antibacterial activities against Gram positive bacteria and Gram negative *Escherichia coli* TolC and a reduced resistance frequency compared to the established antibiotic rifampicin.

© 2013 Elsevier Masson SAS. All rights reserved.

1. Introduction

The bacterial RNA polymerase (RNAP) catalyzes the pivotal transcription process and therefore is an attractive drug target for antibacterial agents [1–3]. Due to its high conservation among a wide range of bacteria, inhibitors of the RNAP are applicable against a broad spectrum of bacterial pathogens [4]. The architecture of the bacterial enzyme significantly differs from eukaryotic RNAP, facilitating a selective blockade of the essential bacterial cell function [5,6]. This is exemplified by a wide range of compounds which selectively effect the prokaryotic RNAP [2]. Several classes of inhibitors targeting bacterial RNAP are known [1,3]. But at the current state the clinically used compounds are limited to lately approved fidaxomicin and members of the rifamycin family [2,7]. For example rifampicin is used in combination with other antibacterials, in the first line therapy of tuberculosis [3,8]. In the meantime some resistant strains, including multi-resistant *Mycobacterium tuberculosis*, emerged [4,9,10]. This creates an urgent need for the development of new classes of antibacterial agents [2,5,11].

A promising strategy to face resistance is the exploration of novel target sites [6,12]. Recently, the “switch region” has been

discovered as an interesting new binding domain of bacterial RNAP [2,4]. Myxopyronin B (**1**), a natural α -pyrone antibiotic isolated from the myxobacterium *Myxococcus fulvus* [13], and its synthetic derivative desmethyl myxopyronin B (**2**) [14], have been demonstrated to target this region [4,15]. Due to the different binding mode compared to the rifamycin antibiotics, compounds binding to the “switch region” are expected to overcome existent resistance [4]. Studies concerning the activity of myxopyronins towards rifamycin-resistant strains of *Staphylococcus aureus* have confirmed, that the “switch region” inhibitors do not exhibit cross-resistance to the rifamycins [16,17]. Although the natural compound myxopyronin B (**1**) is highly active *in vitro* ($IC_{50} = 0.35 \mu\text{M}$; minimal inhibitory concentration = $0.8 \mu\text{g}/\text{mL}$ for *Escherichia coli* TolC), its use as a drug is hampered by insufficient physicochemical properties [18,19]. Therefore small molecule inhibitors possessing a higher *in vivo* efficacy should be developed.

Another project of our group is focused on the optimization of novel RNAP inhibitors of the benzamidobenzoic acid type, identified by a virtual screening, based on the flexible alignment of known inhibitors. Besides good *in vitro* activity these compounds also possess antibacterial effects [20]. In a previous study Fishwick et al. developed inhibitors of bacterial RNAP, using a structure-based *de novo* design approach. These compounds, predicted to bind to the “switch region”, possessed inhibitory activity against *E. coli* RNAP, but displayed no antibacterial properties [21]. Very

* Corresponding author. Tel.: +49 681 302 70300.

E-mail addresses: rolf.hartmann@helmholtz-hzi.de, rwh@mx.uni-saarland.de (R.W. Hartmann).

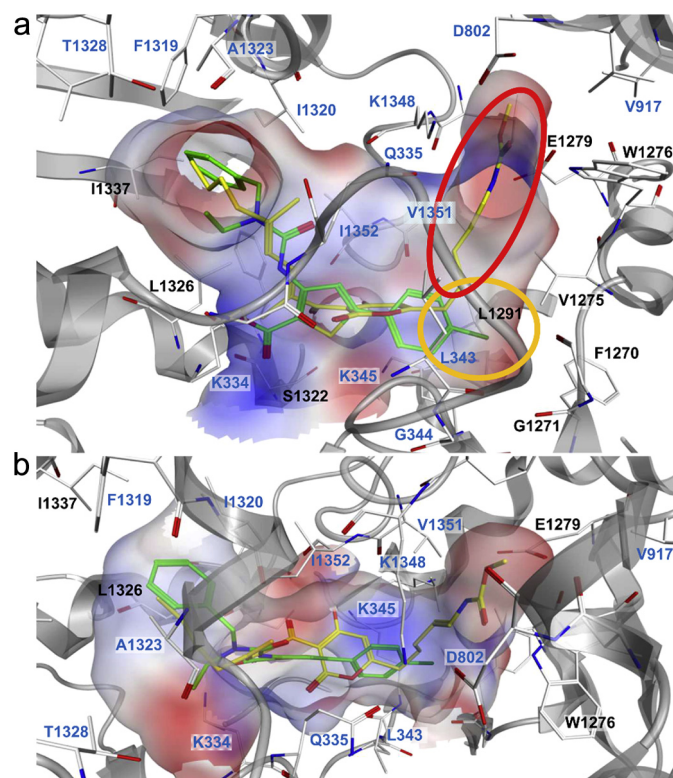


Fig. 1. Binding mode of desmethyl myxopyronin **2** (yellow) and compound **3** (green) at front- (a) and top-view (b). (For interpretation of the references to colour in this figure legend, the reader is referred to the web version of this article.)

recently Buurmann et al. reported on the first synthetic RNAP inhibitors which have been shown to target the “switch region”. Although these compounds were highly active (IC_{50} as low as 4.4 μ M), they showed only weak antibacterial effects [22]. In a further work compounds supposed to interact with the “switch region” were identified by virtual screening, but the putative hits were not experimentally validated [23].

Recently, we identified novel RNAP inhibitors also following a virtual screening approach. A homology model of *E. coli* RNAP was used to set up a 3D-pharmacophore model, which included ligand features from **1** and **2**, but also protein-derived characteristics, matching the “switch region”. Finally, a pharmacophore-based virtual screening of the Chemotheque Nationale library (~42,000 compounds) was performed resulting in a selection of 70 virtual hits. *In vitro* activity determination using an *E. coli* RNAP inhibition assay led to the identification of hit compound **3** showing a moderate inhibitory activity with an IC_{50} value of 75 μ M and MIC value of 11 μ g/mL (*E. coli* TolC) [24]. Interestingly, the related ureido cyclooctathiophenes reported by Arhin et al. for example the acid **5** and especially the esters **6** and **7** have been described to inhibit *S. aureus* RNAP, but their binding site was not further investigated. They showed antibacterial effects against several *S. aureus* strains but not against other Gram positive or Gram negative bacteria [25]. As we expect our compounds to bind to the “switch region” of RNAP, which is highly conserved among various bacterial strains [4], we considered compound **3** to be a good starting point for the development of novel antibacterials with broad spectrum activity.

2. Molecular modeling and optimization strategy

To find out whether the SAR of the ureido cyclooctathiophenes is reasonable to be considered in our study, compounds **5**, **6** and **7**

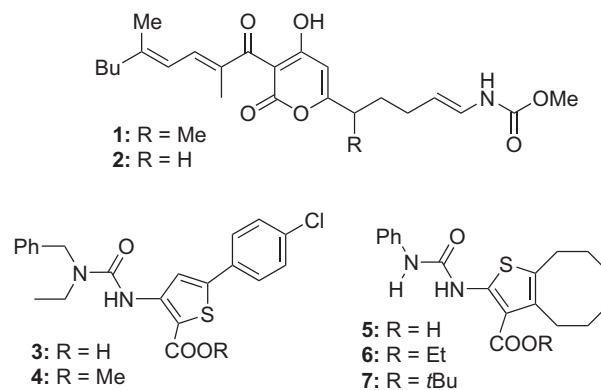


Chart 1. Myxopyronins **1** and **2**, hit compound **3**, its ester **4** and *S. aureus* RNAP inhibitors **5**, **6** and **7**.

were subjected to the virtual screening using our 3D-pharmacophore model. None of them was recognized. This is in accordance with the observation of Buurmann et al. that these ureido cyclooctathiophenes failed to dock to the “switch region” of the RNAP [22]. In both crystal structures of *Thermus thermophilus* RNAP with **1** (PDB ID: 3DXJ) [4] and **2** (PDB ID: 3EQL) [15] the myxopyronins adopt a U-shaped conformation filling the “switch region” binding pocket. According to the docking pose (Fig. 1) hit compound **3** is predicted to bind in a tilted conformation. The thiophene core is placed on the top of the entrance to the switch-2 binding cavity, anchored by atomic interactions (H-bond or ion-pair) of its carboxylic acid moiety with Lys334. Such an interaction is not possible with the corresponding ester **4**. The 4-chlorophenyl ring occupies the lower part of the enecarbamate-binding pocket of myxopyronins. Thereby, the chloro atom is fitted into a small negatively-charged site delimited by Leu343, Gly344 and Lys345 (β' subunit) at one side, and Phe1270, Gly1271, Val1275 and Leu1291 (β subunit) on the other side (red area of the electrostatic potential surface in the orange circle in Fig. 1a) The ureido moiety, stabilized by an intramolecular hydrogen-bond (Chart 2) with the carboxylic acid group, overlaps with the dienone side chain of myxopyronins, pointing the lipophilic substituents ethyl and benzyl into the hydrophobic pocket delimited by Leu1326 and Ile1337 (β subunit) and Phe1319, Ile1320, Ala1323, Thr1328, Ile1352 (β' subunit). Based on this binding mode, **3** was divided into the carboxy–thiophene core and two variable fragments for structure–activity exploration and optimization: the substituted phenyl ring (A), and the ureido group (B) as depicted in chart 2.

3. Chemistry

The synthesis of the 5-aryl-3-ureidothiophene-2-carboxylic acids (Scheme 1) started from readily available acetophenones (**I**) which were converted to the 5-aryl thiophene anthranilic acid

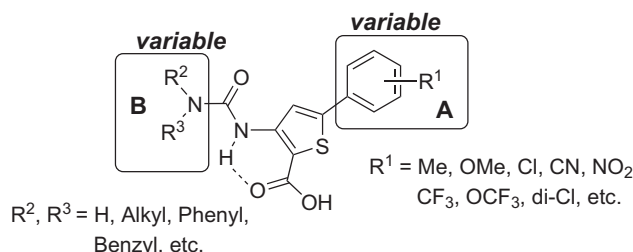
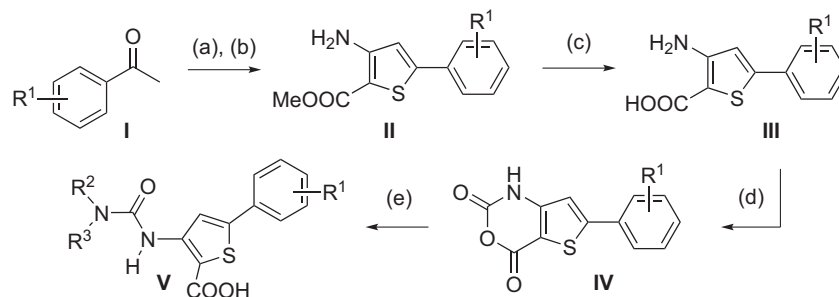


Chart 2. Optimization strategy of 5-aryl-3-ureidothiophene-2-carboxylic acids.



Scheme 1. Synthesis of 5-aryl-3-ureidothiophene-2-carboxylic acids (**V**). Reagents and conditions: (a) POCl_3 , DMF, 50°C to rt, then $\text{NH}_2\text{OH}\cdot\text{HCl}$, up to 150°C , 75–90%. (b) Methylthioglycolate, NaOMe , MeOH , reflux, 65–85%. (c) KOH , MeOH , THF , H_2O , reflux, 40–80%. (d) COCl_2 , THF , 50–70%. (e) Amine, H_2O , 100°C then at 0°C conc. HCl , 40–80%.

methylesters (**II**) via an Arnold–Vilsmaier–Haack reaction followed by a cyclization using methylmercaptoacetate [26]. The esters (**II**) were then hydrolysed under basic conditions to afford the thiophene anthranilic acids (**III**) which were converted into the thiasatoic anhydrides (**IV**) [27,28]. The anhydrides (**IV**) were reacted with various primary and secondary amines giving rise to the 5-aryl-3-ureidothiophene-2-carboxylic acids (**V**) [29]. Compounds **5**, **6** and **7** were synthesized as previously described [25]. Compound **4** was obtained by methylation of compound **3**.

4. Results and discussion

As expected, the ester of **3**, compound **4** did not show *E. coli* RNAP inhibition. Interestingly, not only the esters **6** and **7**, but also the free acid **5** were inactive (Table S2 in Supporting information). During the hit optimization process of the discovered 5-phenyl-3-ureidothiophene-2-carboxylic acids, two aims were pursued: Firstly, the putative binding mode of hit compound **3** was investigated by chemical modifications of the substituents on ring **A**. Thereby the Topliss' logical was followed to optimize the hydrophobic and electronic effects [30]. Secondly, the hydrophobic pocket of the “switch region”, occupied by the dienone side chain of myxopyronins, was explored by varying the substitution pattern of the ureido moiety **B**.

The removal of the chlorine (ring **A**) decreased activity as well as its exchange by a methoxy or methyl group. The introduction of the strongly electron-withdrawing and lipophilic trifluoromethyl group was accompanied by a slight increase in activity. Whereas a more hydrophilic, electron-withdrawing nitro group (**12**) was tolerated, but did not enhance the activity, a cyano group at the same position (**13**) led to a decreased inhibitory effect. An additional chloro substituent improved activity independent of the position of both substituents. This correlates well with the distribution of favorable interaction contour plots for chloro atoms within the subpocket of the “switch region” as computed with Molecular Operating Environment (MOE) [31] (Fig. 2) localized close to positions 2, 3 and 4. The most active compounds in this series were the 3,4-di-chloro compound **18** and **22** with a trifluoromethyl and a chloro substituent present in positions 3 and 4. Regarding quantitative structure–activity relationship (QSAR) an excellent correlation was observed when π and σ were used in a multiparameter regression analysis. The obtained Hansch equation (Equation (1): $\text{pIC}_{50} = 3.71 + 0.34 \times \pi + 0.60 \times \sigma$ ($n = 16$, $R^2 = 0.95$, $\text{RMSE} = 0.071$)) clearly indicates that highly lipophilic and strongly electron-withdrawing groups result in the most potent compounds (Fig. 3).

In order to elucidate the influence of the substitution pattern of ring **A** on the inhibitory potency, *ab initio* geometry optimizations for compounds **3**, **9**, **13** and **18** were carried out and molecular electrostatic potentials (MEP) were visualized (Fig. 4). As shown by

a larger blue area on ring **A** the electrostatic potential was less negative for the potent compound **18**, followed by **13**, **3** and the inactive compound **9**. As seen in the docking poses of compounds **3** and **18** ring **A** is sandwiched between Leu343, Val1351, Ile1352 and the alkyl chain of Lys345, almost perpendicular to the α -pyrone ring of myxopyronin (Figs. 1 and 5). $\text{CH}\text{--}\pi$ and van der Waals interactions are formed between ring **A** and these residues. The introduction of inductive electron-withdrawing substituents on ring **A** leads to a less polarized/negative potential as shown in the MEP maps (progressively less negative potential – Fig. 4). The increase in potency seen for electron-withdrawing groups might depend on stronger London dispersion forces resulting from more balanced electron redistribution at both sides of the ring. The fact that lipophilic (e.g. Cl , CF_3) substituents outreach hydrophilic ones (e.g. CN) fits well with the presence of several apolar residues in the surrounding, i.e. Phe1270, Val1275, Leu1291, Val1351, Ile1352, Val1353 (Fig. 2).

Within the small negatively-charged subpocket (Fig. 1 (orange circle) and Fig. 2) the chloro derivatives **3** and especially **18** are favored due to a complementary electrostatic surface (blue at chloro atom). The more negative potential (green at nitrogen or oxygen) on the methoxy in **9** and cyano group in **13** probably causes electrostatic repulsions and is consequently associated with a drop in activity. Subsuming, the substitution pattern of ring **A** finetunes charge density distribution of the phenyl system and the thiophene core, enabling enhanced interactions with the target protein.

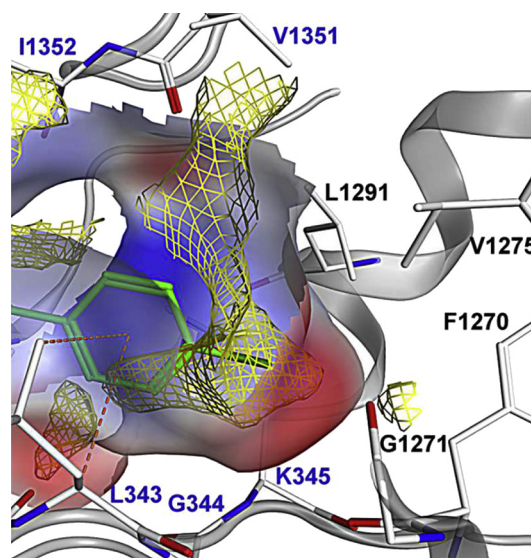


Fig. 2. Small subpocket of the “switch region” with contour graphics (yellow grid) indicating regions where chlorine has interaction energies within isovalues of -4 kcal/mol. (For interpretation of the references to colour in this figure legend, the reader is referred to the web version of this article.)

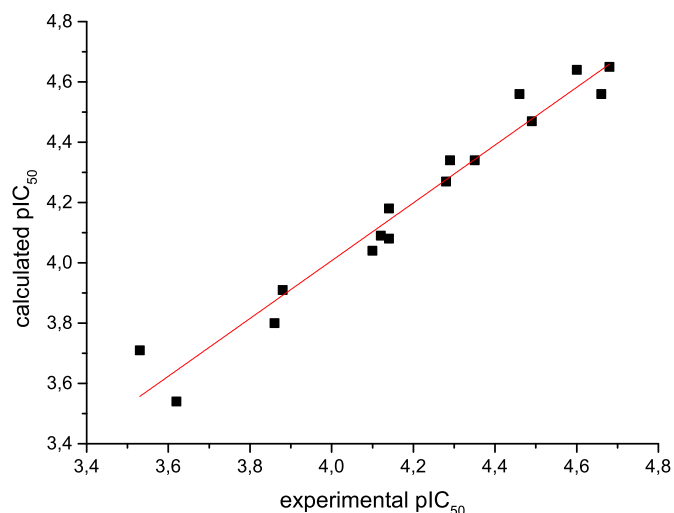


Fig. 3. Comparison of experimentally determined and calculated activities (based on Equation (1)) of compounds **3** and **8–22**.

To proof the binding mode proposed in Fig. 1, compound **23** was synthesized [40]. It was deduced from the docking pose, that position 3 at the phenyl ring **A** should be appropriate for an elongation into the pocket occupied by the enecarbamate chain of myxopyronins (red circle in Fig. 1). As a linker a C_4 unit has been considered to be suitable for the positioning of a carbamate group. For synthetic reasons we introduced a saturated chain as the corresponding myxopyronin analogue has been described to show a similar biological activity as **1** [14]. The resulting compound **23** that contains a mimic of the myxopyronin enecarbamate chain indeed possessed increased activity compared to the parent compound **3** (Table 2). Nevertheless the putative new interactions (Figure S2 in Supporting information) would suggest an even higher gain in activity. We suppose that the entropic penalty for the binding of the highly flexible chain has a negative effect on the affinity. Furthermore, it can be rationalized that the positive inductive effect of the introduced alkylcarbamate chain negatively affects the electronic properties of ring **A** according to equation (1). The fact that **23** is

more active than **3**, despite these two negative effects, corroborates the validity of the docking pose.

Turning our interest to the ureido motif **B**, we retained the 3,4-di-chloro ring **A**. The unsubstituted ureido compound **24** ($R^2 = R^3 = H$) displayed low affinity compared to **18** containing two lipophilic alkyl chains. This was concordant with the proposed binding mode since **B** is located in a highly lipophilic cavity where hydrophobic contacts, Van der Waals and $CH-\pi$ interactions, prevail. As depicted in Fig. 5 the urea moiety does not form hydrogen-bonds with surrounding residues, but acts as a planar linker for the obligatory hydrophobic groups. Within the compound series derived from primary alkyl amines an increased activity was observed for chain elongation. For example the *n*-hexyl derivative **28** displayed the highest potency compared to smaller substituents. Besides long aliphatic chains, aromatic residues (phenyl, benzyl or phenethyl) were also suitable. The introduction of a second chain at the nitrogen was in general accompanied by an increasing activity.

The increase in potency of compounds **35–40** compared to the mono-substituted derivatives **29–31** appears to rely on additional hydrophobic contacts within the lipophilic pocket. In fact these compounds present a second sterically demanding, hydrophobic substituent at the ureido motif (**B**). These moieties better fill the dienone-binding cavity reaching into the pocket delimited by Leu1326 and Ile1330 (β subunit), and Lys332, Ser1324, Thr1328, and Leu1332 (β' subunit). For instance, the higher affinity of **40** can be explained by additional $CH-\pi$ interactions between the second aromatic ring and Lys334 (β' subunit) as well as by non-bonded interactions with Leu1332 and Thr1328, whereas compound **18** only interacts with Ile1320 and Leu1326 in the dienone pocket (Fig. 5). Subsuming, the increase of activity by extension of the lipophilic side chains in part **B** can be attributed to a better fit into the binding cavity and therefore extension of the hydrophobic contact area and displacement of water molecules.

In addition to the RNAP *in vitro* inhibition, the effect of **18** on RNA synthesis was investigated in a whole-cell assay with *E. coli* TolC using radiolabeled 3H uridine. At a concentration of 100 μM the RNA level was reduced by 60% after 40 min (Figure S2).

Further biological evaluation was carried out by determination of minimal inhibitory concentrations (MIC) in *E. coli* TolC (Table 1), which is defective in the multidrug AcrAB–TolC efflux system. Most

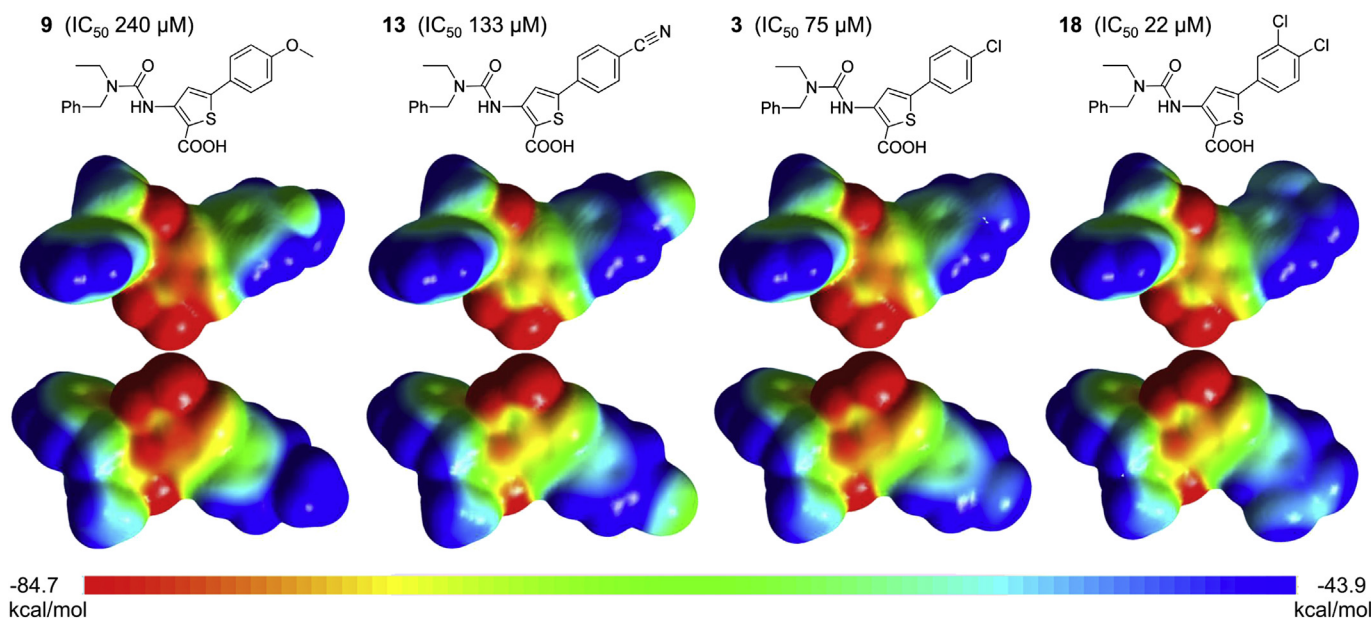


Fig. 4. *Ab initio* molecular electrostatic potential (MEP) of compounds **3**, **9**, **13** and **18**.

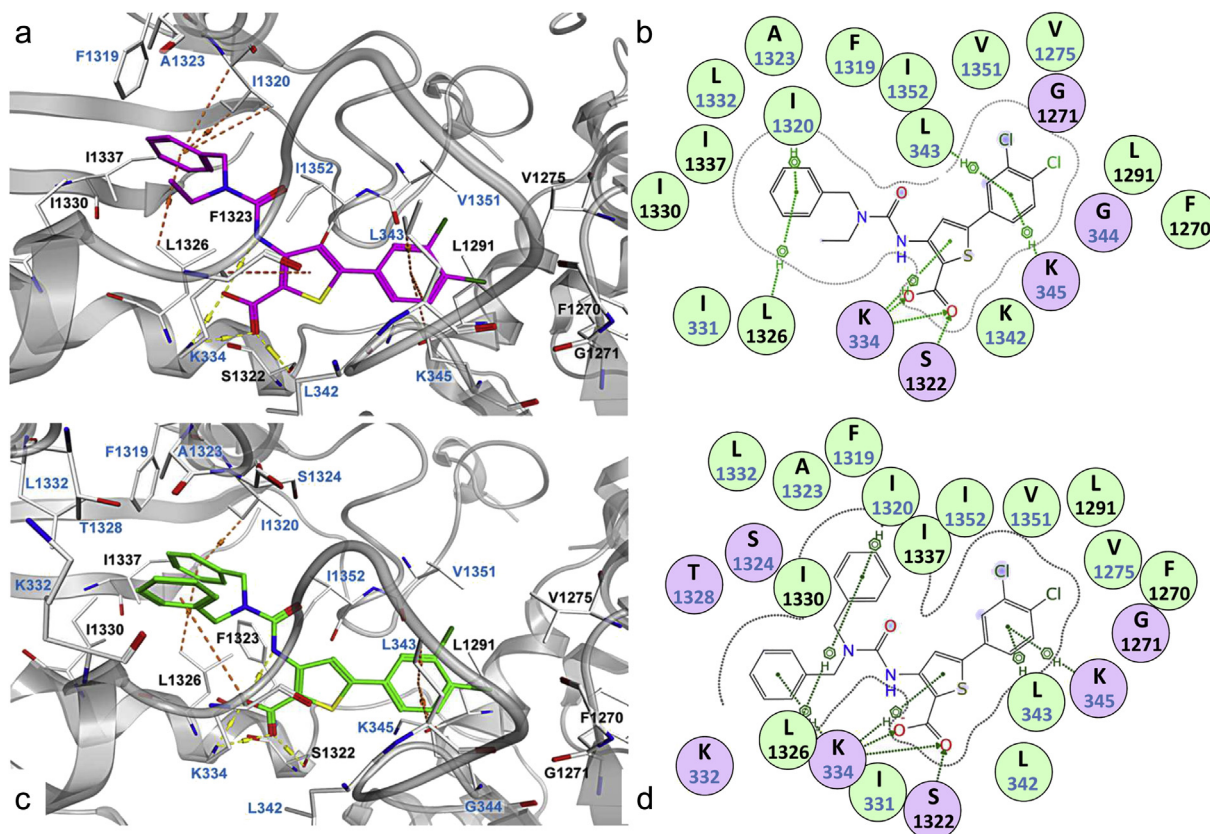


Fig. 5. Docking simulation of compounds **18** (a) and **40** (c) and two-dimensional illustration of the interactions between **18** (b) and **40** (d) and RNAP. The main interacting amino acids and the key interactions are highlighted. Numbers of amino acid residues from β and β' subunit are labeled in black and blue. Polar amino acids are illustrated in purple and hydrophobic amino acids in green circles. (For interpretation of the references to colour in this figure legend, the reader is referred to the web version of this article.)

Table 1
Inhibitory activities against *E. coli* RNA polymerase *in vitro* and antibacterial activities.

| Cpd | R ¹ | Inhibition of <i>E. coli</i> RNAP ^a (μ M) | MIC (μ g/mL) ^{b,c} | Cpd | R ² | R ³ | Inhibition of <i>E. coli</i> RNAP ^a | MIC (μ g/mL) ^{b,c} |
|-----------|--------------------------|---|----------------------------------|-----------|------------------|------------------|--|----------------------------------|
| 3 | 4-Cl | 75 | 11 | 24 | H | H | 26% | >25 |
| 8 | H | 292 | 17 | 25 | H | <i>i</i> -propyl | 26% | 15 |
| 9 | 4-OCH ₃ | 240 | 15 | 26 | H | <i>n</i> -butyl | 91 μ M | 13 |
| 10 | 4-CH ₃ | 137 | 21 | 27 | H | <i>n</i> -pentyl | 35 μ M | 10 |
| 11 | 4-CF ₃ | 51 | 21 | 28 | H | <i>n</i> -hexyl | 19 μ M | >25 |
| 12 | 4-NO ₂ | 73 | 23 | 29 | H | Phenyl | 25 μ M | 12 |
| 13 | 4-CN | 133 | 25 | 30 | H | Benzyl | 45 μ M | 10 |
| 14 | 4-OCF ₃ | 45 | 21 | 31 | H | Phenethyl | 26 μ M | 8 |
| 15 | 3-Cl | 72 | 9 | 32 | Methyl | Phenyl | 45 μ M | 9 |
| 16 | 3-CF ₃ | 53 | 38 | 33 | Methyl | Benzyl | 12% | 5 |
| 17 | 3-NO ₂ | 80 | 22 | 34 | Ethyl | Phenyl | 36 μ M | 16 |
| 18 | 3,4-di-Cl | 22 | 10 | 18 | Ethyl | Benzyl | 22 μ M | 10 |
| 19 | 2,4-di-Cl | 32 | 8 | 35 | <i>n</i> -propyl | Benzyl | 14 μ M | >25 |
| 20 | 2,5-di-Cl | 35 | 9 | 36 | <i>n</i> -propyl | Phenethyl | 12 μ M | >25 |
| 21 | 3,5-di-Cl | 25 | n.d. | 37 | <i>n</i> -butyl | Phenyl | 14 μ M | >25 |
| 22 | 3-CF ₃ , 4-Cl | 21 | 12 | 38 | <i>n</i> -butyl | Benzyl | 9 μ M | >50 |
| 1 | Myxopyronin B | 0.35 | 0.8 | 39 | <i>n</i> -butyl | Phenethyl | 7 μ M | >25 |
| | Rifampicin | 0.03 | 5 | 40 | Benzyl | Benzyl | 6 μ M | >25 |

^a IC₅₀ values [μ M] or inhibition at 100 μ M [%] of *E. coli* RNA polymerase.

^b Minimal inhibitory concentration in *E. coli* TolC.

^c >: MIC-determination was limited due to insufficient solubility of the tested compounds. n.d. = not determined.

Table 2
Structure and biological data of **23**.

| | |
|--|---|
| <p style="text-align: center;">23</p> | <p>IC₅₀ <i>E. coli</i> RNAP: 20 μM MIC <i>E. coli TolC</i>: 25 μg/mL</p> |
|--|---|

of the compounds active against the bacterial enzyme displayed growth inhibitory effects in the range of 5–25 μg/mL. Their antibacterial activity is comparable to that of the reference drug rifampicin (5 μg/mL *E. coli TolC*). The effect on the bacterial growth reflects that the ureidothiophene carboxylic acids can diffuse across the asymmetric bilayer to gain access to the cell interior, as described for lipophilic antibacterials including macrolides and rifamycins [32]. However, the most potent RNAP inhibitors **35–40** – the compounds with the highest lipophilicity in that class – showed lower antibacterial potency against *E. coli TolC*. These results can be explained by the fact that the outer membrane of Gram negative bacteria is well known to be a potent barrier, hindering too lipophilic compounds from entering the cell [33,34].

To explore the spectrum of bacteria possessing susceptibility to selected compounds, MIC values in two Gram positive and two Gram negative strains were determined (Table 3). While the Gram positive strains (*Bacillus subtilis*, *S. aureus*) were in general sensitive, wild type Gram negative bacteria (*E. coli K12*, *Pseudomonas aeruginosa*) were not affected. For *B. subtilis* and *S. aureus* similar inhibitory effects compared to *E. coli TolC* were observed. Considering that the RNAP “switch region” is highly conserved among various bacterial strains, we assume that the unequal antibacterial potencies are due to differences in cell wall permeability between Gram negative and Gram positive bacteria.

The fact that most compounds were potent against the *TolC* mutant of *E. coli* and almost ineffective against *E. coli K12* suggests that drug efflux, deactivated in *E. coli TolC*, is responsible for the lack of antibacterial potency in Gram negative bacteria.

An essential requirement for an effective antibacterial agent is that its potency is not reduced by the occurrence of resistant strains. Spontaneous resistance towards myxopyronin B in *S. aureus* occurs at a frequency of 8×10^{-8} , similar to that of rifampicin [17]. The determination of the *in vitro* resistance frequencies in *E. coli TolC* at $2 \times$ MIC revealed a significant (>500-fold) lower value for **15** ($<4.2 \times 10^{-11}$) compared to rifampicin (8.3×10^{-8}) and myxopyronin B (7.1×10^{-8}). This phenomenon can be explained by the fact that **15** occupies only a part of the “switch region” whereas myxopyronin fills a larger area, including the narrow enecarbamate-binding pocket. Especially mutations in this part, which lead to resistance against myxopyronin [4,35], should not affect the antibacterial activity of our compounds. Another mechanism that can contribute to the low resistance frequency can be the effect on an additional target. This will be investigated in further experiments. Our finding indicates, that the probability of occurring resistant strains, is reduced with our compounds compared to existing drugs. This makes these compounds promising candidates for further optimization as novel antibacterials.

5. Conclusions

With the aim to develop antibacterial substances with broad spectrum activity, we have chosen the “switch region” of bacterial RNAP as a target site, as it is conserved among various bacterial strains [4]. In a previous work we had discovered hit compound **3**

Table 3
Antibacterial activities of selected 5-aryl-3-ureidothiophene-2-carboxylic acids.

| Cpd | MIC ^a | MIC ^a | MIC ^a | MIC ^a | MIC ^a |
|---------------|--------------------------------|-------------------------------|---------------------------------|-------------------------------|-----------------------------|
| | <i>E. coli TolC</i> (μg/mL) | <i>E. coli K12</i> (μg/mL) | <i>P. aeruginosa</i> (μg/mL) | <i>B. subtilis</i> (μg/mL) | <i>S. aureus</i> (μg/mL) |
| 14 | 21 | >100 | >100 | 20 | 9 |
| 15 | 9 | >100 | >100 | 12 | 21 |
| 18 | 10 | >25 | >25 | 11 | 8 |
| 19 | 8 | >50 | >50 | 10 | 12 |
| 22 | 12 | >50 | >50 | 20 | 5 |
| 27 | 10 | >25 | >25 | 8 | >25 |
| 29 | 12 | >50 | >50 | 12 | 6 |
| 31 | 8 | >25 | >25 | 7 | 6 |
| 38 | >50 | >50 | >50 | >50 | >50 |
| 40 | >25 | >25 | >25 | >25 | 3 |
| 1 | 0.8 | >25 | >25 | 0.9 | 0.5 |
| Rifampicin | 10 | 7 | 13 | 4.8 | 0.02 |
| Myxopyronin B | 0.8 | >25 | >25 | 0.9 | 0.5 |

^a >: MIC-determination was limited due to insufficient solubility of the tested compounds.

via virtual screening using a 3D-pharmacophore model [24], based on the cocrystal structures of myxopyronin **1** and **2** in the “switch region” [4,15]. In this paper the SAR of compound **3** was explored and the inhibitory potency was optimized following a rational approach (Hansch, Topliss) supported by computational methods (docking studies, MEPs). Furthermore, the binding mode was experimentally validated by mimicking the natural ligand myxopyronin via introduction of a carbamate side chain into compound **3**. The new inhibitors show activity against Gram positive (*B. subtilis*, *S. aureus*) and Gram negative (*E. coli TolC*) bacterial strains accompanied by outstanding low resistance frequencies. In contrast, other synthetic RNAP inhibitors possess weak bacterial growth inhibitory activity [21,22] or have only narrow spectrum activity among the *S. aureus* genus [25]. The lack of activity towards Gram negative wild type strains, is most likely due to poor penetration and/or drug efflux. Therefore further optimization is required. Improving the physicochemical properties by introduction of hydrophilic or ionisable groups could enhance cellular availability in Gram negative bacteria. Ring **A** seems to be inappropriate since Equation (1) shows the importance of lipophilic substituents in this part. In our opinion, the ureido motif **B** is so far underexploited and should be utilized. As it is known, that the introduction of polar groups can have negative impact on the activity unless they contribute to favorable enthalpic interactions [36,37], this issue has to be taken into consideration. In the binding area of **B** the polar amino acids (Ser1324, Thr1328) and some backbone regions could be addressed for such interactions. Thus, clinically applicable, broad spectrum antibacterial agents, that are urgently needed to combat infectious diseases, could finally be obtained. The present work lays the foundation for future structure-based design and expansion of the chemical space in this class.

6. Experimental procedures

6.1. Chemistry

6.1.1. Materials and methods

Starting materials were purchased from commercial suppliers and used without further purification. Column flash chromatography was performed on silica gel (40–63 μm), and reaction progress was monitored by TLC on TLC Silica Gel 60 F₂₅₄ (Merck). All moisture-sensitive reactions were performed under nitrogen atmosphere using oven-dried glassware and anhydrous solvents. ¹H and ¹³C NMR spectra were recorded on a Bruker Fourier

spectrometer (300 or 75 MHz) at ambient temperature with the chemical shifts recorded as δ values in ppm units by reference to the hydrogenated residues of deuteriated solvent as internal standard. Coupling constants (J) are given in Hz and signal patterns are indicated as follows: s, singlet; d, doublet; dd, doublet of doublets; t, triplet; m, multiplet, br., broad signal. The melting points (m.p.) were determined using a Stuart Scientific SMP3. The purity of the final compounds was $\geq 95\%$ as measured by HPLC. The Surveyor LC system consisted of a pump, an autosampler, and a PDA detector. Mass spectrometry was performed on an MSQ electrospray mass spectrometer (ThermoFisher, Dreieich, Germany). The system was operated by the standard software Xcalibur. An RP C18 NUCLEODUR 100-5 (125 mm \times 3 mm) column (Macherey–Nagel GmbH, Düren, Germany) was used as the stationary phase. All solvents were HPLC grade. In a gradient run the percentage of acetonitrile (containing 0.1% trifluoroacetic acid) was increased from an initial concentration of 0% at 0 min to 100% at 15 min and kept at 100% for 5 min. The injection volume was 10 μ L, and flow rate was set to 800 μ L/min. MS analysis was carried out at a spray voltage of 3800 V and a capillary temperature of 350 °C and a source CID of 10 V. Spectra were acquired in positive mode from 100 to 1000 m/z at 254 nm for the UV trace.

6.1.2. General procedure for the synthesis of ureidothiophene-2-carboxylic acids

6.1.2.1. General procedure for the synthesis of 5-aryl-3-amino-2-carboxylic acid methyl ester (II). POCl₃ (26.1 g, 0.17 mol) was added dropwise to DMF (24.9 g, 0.34 mol) maintaining the temperature beyond 25 °C (cooling in ice bath) and stirred for additional 15 min. The acetophenone **I** (85.0 mmol) was added slowly and the temperature was kept between 40 and 60 °C. After complete addition, the mixture was stirred for 30 min at room temperature. Hydroxylamine hydrochloride (23.6 g, 0.34 mol) was carefully added portionwise (exothermic reaction!) and the reaction was stirred for additional 30 min without heating. After cooling to room temperature, the mixture was poured into ice water (300 mL). The precipitated β -chloro-cinnamionitrile was collected by filtration, washed with H₂O (2 \times 50 mL) and dried under reduced pressure over CaCl₂. In the next step sodium (1.93 g, 84.0 mmol) was dissolved in MeOH (85 mL) and methylthioglycolate (6.97 g, 65.6 mmol) was added to the stirred solution. The β -chloro-cinnamionitrile (61.1 mmol) was added and the mixture was heated to reflux for 30 min. After cooling to room temperature, the mixture was poured into ice water (300 mL). The precipitated solid was collected by filtration, washed with H₂O (2 \times 50 mL) and dried under reduced pressure over CaCl₂. If necessary, recrystallisation from EtOH was performed.

6.1.2.2. General procedure for the synthesis of 5-aryl-3-amino-2-carboxylic acid (III). The 5-aryl-3-amino-2-carboxylic acid methyl ester (16.6 mmol) was added to a solution of KOH (60 mL, 0.6 M in H₂O) and MeOH (60 mL). The mixture was heated to reflux for 3 h, concentrated, and washed with EtOAc (2 \times 50 mL). The aqueous layer was cooled with ice and acidified by addition of a saturated aqueous solution of KHSO₄. The precipitated solid was collected by filtration, washed with H₂O (2 \times 30 mL) and dried under reduced pressure over CaCl₂.

6.1.2.3. General procedure for the synthesis of 5-aryl-2-thiaisoic-anhydrid (IV). To a solution of the 5-aryl-3-amino-2-carboxylic acid (III) (5.28 mmol) in THF (50 mL) a solution of phosgene (6.10 mL, 20 wt% in toluene, 11.6 mmol) was added dropwise over a period of 30 min. The reaction mixture was stirred for 2 h at room temperature, followed by the addition of saturated aqueous

solution of NaHCO₃ (30 mL) and H₂O (50 mL). The resulting mixture was extracted with EtOAc/THF (1:1, 3 \times 100 mL). The organic layer was washed with saturated aqueous NaCl (100 mL), dried (MgSO₄) and concentrated. The crude material was suspended in a mixture of *n*-hexane/EtOAc (2:1, 50 mL) heated to 50 °C and after cooling to room temperature separated via filtration.

6.1.2.4. General procedure for the synthesis of 5-aryl-3-ureidothiophene-2-carboxylic acid (V). The 5-aryl-2-thiaisoic-anhydrid (IV) (0.46 mmol) was suspended in water (7.5 mL) and the appropriate amine (4.60 mmol) was added. The reaction mixture was stirred, heated to 100 °C and then cooled to room temperature. The reaction mixture was poured into a mixture of concentrated HCl and ice (1:1) and extracted with EtOAc/THF (1:1, 60 mL). The organic layer was washed with aqueous HCl (2 M), followed by saturated aqueous NaCl (2 \times 50 mL), dried (MgSO₄) and concentrated. The crude material was suspended in a mixture of *n*-hexane/EtOAc (2:1, 20 mL) heated to 50 °C and after cooling to room temperature separated via filtration.

6.1.3. Spectroscopic data of final compounds

Spectroscopic data of final compounds can be found in the [Supporting information](#). Compound **3** is presented as example.

6.1.3.1. 5-(4'-chlorophenyl)-3-[(N-ethylbenzylamino)carbonylamino]-thiophene-2-carboxylic acid (3). Yellow powder, m.p. 173–174 °C.

¹H NMR (300 MHz, DMSO-*d*₆): δ = 1.16 (t, J = 7.1 Hz, 3H), 3.39 (q, J = 7.1 Hz, 2H), 4.58 (s, 2H), 7.24–7.38 (m, 5H), 7.50 (d, J = 8.5 Hz, 2H), 7.71 (d, J = 8.5 Hz, 2H), 8.29 (s, 1H), 10.06 (s, 1H), 13.40 (br. s, 1H, COOH) ppm.

¹³C NMR (75 MHz, DMSO-*d*₆): δ = 13.1, 41.8, 49.3, 107.2, 117.8, 127.1, 127.1, 127.4, 128.5, 129.3, 131.5, 133.8, 138.1, 146.1, 146.7, 153.0, 165.6 ppm.

6.2. Biology

6.2.1. Transcription assay

E. coli RNA polymerase holo enzyme was purchased from Epicentre Biotechnologies (Madison, WI). Final concentrations in a total volume of 30 μ L were one unit of RNA polymerase (0.5 μ g) which were used along with 60 nCi of [5,6-³H]-UTP, 400 μ M of ATP, CTP and GTP as well as 100 μ M of UTP, 20 units of RNase inhibitor (RiboLock, Fermentas), 10 mM DTT, 40 mM Tris–HCl (pH 7.5), 150 mM KCl, 10 mM MgCl₂ and 0.1% CHAPS. As a DNA template 3500 ng of religated pcDNA3.1/V5-His-TOPO were used per reaction [38]. Prior to starting the experiment, the compounds were dissolved in DMSO (final concentration during experiments: 2%). Dilution series of compounds were prepared using a liquid handling system (Janus, Perkin Elmer, Waltham, MA). The components described above (including the inhibitors) were preincubated in absence of NTPs and DNA for 10 min at 25 °C. Transcription reactions were started by the addition of a mixture containing DNA template and NTPs and incubated for 10 min at 37 °C. The reaction was stopped by the addition of 10% TCA, followed by a transfer of this mixture to a 96-well Multiscreen GFB plate (Millipore, Billerica, MA) and incubation for 45 min at 4 °C. The plate underwent several centrifugation and washing steps with 10% TCA and 95% ethanol to remove residual unincorporated ³H UTP. After that the plate was dried (30 min, 50 °C) and 30 μ L of scintillation fluid (Optiphase Supermix, Perkin Elmer) was added to each well. After 10 min the wells were assayed for presence of ³H RNA by counting using a Wallac MicroBeta TriLux system (Perkin Elmer). To obtain inhibition values for each sample, their counts were related to DMSO controls.

6.2.2. RNA synthesis assay

E. coli TolC was cultured in lysogeny broth (LB) medium. ^3H uridine (1 $\mu\text{Ci}/\text{mL}$) was added during the logarithmic growth phase and 3 min before the addition of compound **18** at 100 μM (0.5% DMSO). 300 μL of the cultured bacteria were harvested 40 min after addition of the inhibitors and supplemented with 2 volumes of 10% TCA. After 45 min at 4 °C the precipitates were collected and washed using a 96-well glass fiber filter plate (Multiscreen GFB) (Millipore, Billerica, MA). After adding Optiphase Supermix (Perkin Elmer, Waltham, MA) the quantification of radioactivity was performed using a Wallac MicroBeta TriLux system (Perkin Elmer).

6.2.3. Determination of IC_{50} values

For the determination of IC_{50} values three different concentrations of a compound were chosen (two samples for each concentration) including data points above and below the IC_{50} value. The calculation of the IC_{50} value was performed by plotting the percent inhibition vs. the concentration of inhibitor on a semi-log plot. From this the molar concentration causing 50% inhibition was calculated. At least three independent determinations were performed for each compound.

6.2.4. Minimal inhibitory concentration (MIC) determinations

MIC values in *E. coli TolC* were performed with all compounds. Selected compounds were additionally tested in *E. coli K12*, *B. subtilis* subsp. *subtilis*, *P. aeruginosa PAO1* and *S. aureus* subsp. *aureus* (Newman strain). As a bacteria start OD_{600} 0.03 was used in a total volume of 200 μL in lysogeny broth (LB) containing the compounds predissolved in DMSO (maximal DMSO concentration in the experiment: 1%). Final compound concentrations prepared from serial dilutions ranged from 0.02 to 100 $\mu\text{g}/\text{mL}$ (double values for each concentration) depending on their antibacterial activity and the observation of compound precipitation in the growth medium. The ODs were determined after addition of the compounds and again after incubation for 18 h at 37 °C and 50 rpm (200 rpm for *PAO1*) in a 96-well plates (Sarstedt, Nümbrecht, Germany) using a FLUOStar Omega (BMG labtech, Ortenberg, Germany). Given MIC values are means of two independent determinations (three if $\text{MIC} < 10 \mu\text{g}/\text{mL}$) and are defined as concentrations at which bacterial growth was no more detectable.

6.2.5. Determination of resistance frequency

The amount of *E. coli TolC* cells per mL was determined by plating bacteria dilutions on LB agar plates following colony counting. Different amounts of cells were incubated in LB in presence of the $2 \times \text{MIC}$ of rifampicin, myxopyronin B and compound **18** in parallel (16 h, 37 °C, 50 rpm) following LB exchange, recultivation and growth control. A threshold was determined at which bacterial growth and hence resistance development occurred following calculation of the resistance frequency.

6.3. Computational chemistry

6.3.1. Docking calculations

Selected compounds were docked into the switch region of the *E. coli* RNAP homology model using Goldv5.0 [24].

6.3.2. Molecular electrostatic potential

For compounds **3**, **9**, **13**, and **18** *ab initio* geometry optimizations were performed choosing as basis set HF/6-31+ G (d,p) by means of the Gaussian 03 software, and the molecular electrostatics potential map (MEP) was plotted using GaussView, version 3.0, the 3D molecular graphics package of Gaussian [39]. Electrostatic potential surfaces were generated mapping the electrostatic potentials onto molecular electron densities at an isovalue of 0.0004 $e/\text{Å}^3$. The MEP maps are color-coded, ranging from -85 (red) to -44 (blue) kcal/mol.

6.3.3. QSAR model

The QSAR model (Equation (1)) was obtained using the software Molecular Operating Environment (MOE) v. 2010.10.

Acknowledgments

The authors thank Jeannine Jung and Jannine Ludwig for performing the *in vitro* tests. We also appreciate Ailke Gerstner for her help in performing the synthesis. Furthermore we are grateful to K. Gerth (Helmholtz Centre for Infection Research (HZI) in Braunschweig) for kindly providing myxopyronin B. J. Henning Sahner gratefully acknowledges a scholarship from the “Stiftung der Deutschen Wirtschaft” (SDW).

Appendix A. Supplementary data

Supplementary data related to this article can be found at <http://dx.doi.org/10.1016/j.ejmech.2013.04.060>.

References

- [1] A. Srivastava, M. Talaue, S. Liu, D. Degen, R.Y. Ebright, E. Sineva, A. Chakraborty, S.Y. Druzhinin, S. Chatterjee, J. Mukhopadhyay, Y.W. Ebright, A. Zozula, J. Shen, S. Sengupta, R.R. Niedfeldt, C. Xin, T. Kaneko, H. Irschik, R. Jansen, S. Donadio, N. Connell, R.H. Ebright, New target for inhibition of bacterial RNA polymerase: 'switch region', *Curr. Opin. Microbiol.* 14 (2011) 532–543.
- [2] I. Chopra, Bacterial RNA polymerase: a promising target for the discovery of new antimicrobial agents, *Curr. Opin. Invest. Drugs* 8 (2007) 600–607.
- [3] R. Mariani, S.I. Maffioli, Bacterial RNA polymerase inhibitors: an organized overview of their structure, derivatives, biological activity and current clinical development status, *Curr. Med. Chem.* 16 (2009) 430–454.
- [4] J. Mukhopadhyay, K. Das, S. Ismail, D. Koppstein, M. Jang, B. Hudson, S. Sarafianos, S. Tuske, J. Patel, R. Jansen, H. Irschik, E. Arnold, R.H. Ebright, The RNA polymerase “switch region” is a target for inhibitors, *Cell* 135 (2008) 295–307.
- [5] P. Cramer, Multisubunit RNA polymerases, *Curr. Opin. Struct. Biol.* 12 (2002) 89–97.
- [6] R.H. Ebright, RNA polymerase: structural similarities between bacterial RNA polymerase and eukaryotic RNA polymerase II, *J. Mol. Biol.* 304 (2000) 687–698.
- [7] I. Artsimovitch, J. Seddon, P. Sears, Fidaxomicin is an inhibitor of the initiation of bacterial RNA synthesis, *Clin. Infect. Dis.* 55 (Suppl. 2) (2012) S127–S131.
- [8] T. Schaberg, M. Forßbohm, B. Hauer, D. Kirsten, R. Kropp, R. Loddenkemper, K. Magdorf, H. Rieder, D. Sagebiel, R. Urbanczik, Richtlinien zur medikamentösen Behandlung der Tuberkulose im Erwachsenen- und Kindesalter, *Pneumologie* 55 (2001) 494–511.
- [9] A. Pablos-Méndez, M.C. Raviglione, A. Laszlo, N. Binkin, H.L. Rieder, F. Bustreo, D.L. Cohn, C.S. Lambregts-van Weezenbeek, S.J. Kim, P. Chaulet, P. Nunn, Global surveillance for antituberculosis-drug resistance, 1994–1997. World Health Organization—International Union against tuberculosis and Lung disease working group on anti-tuberculosis drug resistance surveillance, *N. Engl. J. Med.* 338 (1998) 1641–1649.
- [10] M.A. Espinal, A. Laszlo, L. Simonsen, F. Boulahbal, S.J. Kim, A. Reniero, S. Hoffner, H.L. Rieder, N. Binkin, C. Dye, R. Williams, M.C. Raviglione, Global trends in resistance to antituberculosis drugs. World Health Organization—International Union against tuberculosis and lung disease working group on anti-tuberculosis drug resistance surveillance, *N. Engl. J. Med.* 344 (2001) 1294–1303.
- [11] L.B. Rice, Unmet medical needs in antibacterial therapy, *Biochem. Pharmacol.* 71 (2006) 991–995.
- [12] Q. Al-Balas, N.G. Anthony, B. Al-Jaidi, A. Alnimr, G. Abbott, A.K. Brown, R.C. Taylor, G.S. Besra, T.D. McHugh, S.H. Gillespie, B.F. Johnston, S.P. Mackay, G.D. Coxon, Identification of 2-aminothiazole-4-carboxylate derivatives active against *Mycobacterium tuberculosis* H37Rv and the β -ketoacyl-ACP synthase mtFabH, *PLoS ONE* 4 (2009) e5617.
- [13] H. Irschik, K. Gerth, G. Höfle, W. Kohl, H. Reichenbach, The myxopyronins, new inhibitors of bacterial RNA synthesis from *Myxococcus fulvus* (Myxobacterales), *J. Antibiot.* 36 (1983) 1651–1658.
- [14] T. Doundoulakis, A.X. Xiang, R. Lira, K.A. Agrios, S.E. Webber, W. Sisson, R.M. Aust, A.M. Shah, R.E. Showalter, J.R. Appleman, K.B. Simonsen, Myxopyronin B analogs as inhibitors of RNA polymerase, synthesis and biological evaluation, *Bioorg. Med. Chem. Lett.* 14 (2004) 5667–5672.
- [15] G.A. Belogurov, M.N. Vassilyeva, A. Sevostyanova, J.R. Appleman, A.X. Xiang, R. Lira, S.E. Webber, S. Klyuyev, E. Nudler, I. Artsimovitch, D.G. Vassilyev, Transcription inactivation through local refolding of the RNA polymerase structure, *Nature* 457 (2009) 332–335.
- [16] A. O'Neill, B. Oliva, C. Storey, A. Hoyle, C. Fishwick, I. Chopra, RNA polymerase inhibitors with activity against rifampin-resistant mutants of *Staphylococcus aureus*, *Antimicrob. Agents Chemother.* 44 (2000) 3163–3166.

- [17] T.I. Moy, A. Daniel, C. Hardy, A. Jackson, O. Rehrauer, Y.S. Hwang, D. Zou, K. Nguyen, J.A. Silverman, Q. Li, C. Murphy, Evaluating the activity of the RNA polymerase inhibitor myxopyronin B against *Staphylococcus aureus*, *FEMS Microbiol. Lett.* 319 (2011) 176–179.
- [18] D. Haebich, F. von Nussbaum, Lost in transcription – inhibition of RNA polymerase, *Angew. Chem. Int. Ed.* 48 (2009) 3397–3400.
- [19] R. O'Shea, H.E. Moser, Physicochemical properties of antibacterial compounds: implications for drug discovery, *J. Med. Chem.* 51 (2008) 2871–2878.
- [20] S. Hinsberger, M. Groh, M. Negri, J. Hauptenthal, R.W. Hartmann, unpublished results.
- [21] M.J. McPhillie, R. Trowbridge, K.R. Mariner, A.J. O'Neill, A.P. Johnson, I. Chopra, C.W.G. Fishwick, Structure-based ligand design of novel bacterial RNA polymerase inhibitors, *ACS Med. Chem. Lett.* 2 (2011) 729–734.
- [22] E.T. Buurman, M.A. Foulk, N. Gao, V.A. Laganas, D.C. McKinney, D.T. Moustakas, J.A. Rose, A.B. Shapiro, P.R. Fleming, Novel rapidly diversifiable antimicrobial RNA polymerase switch region inhibitors with confirmed mode of action in *Haemophilus influenzae*, *J. Bacteriol.* 194 (2012) 5504–5512.
- [23] Y.S. Li, L. Zhou, X. Ma, H. Song, X.Y. Tang, Pharmacophore modeling and structure-based virtual screening for a novel “switch region” target of bacterial RNA polymerase, *Med. Chem. Res.* (2011) 1–11.
- [24] M. Negri, J. Hauptenthal, R.W. Hartmann, unpublished results.
- [25] F. Arhin, O. Bélanger, S. Ciblat, M. Dehbi, D. Delorme, E. Dietrich, D. Dixit, Y. Lafontaine, D. Lehoux, J. Liu, G.A. McKay, G. Moeck, R. Reddy, Y. Rose, R. Srikumar, K.S.E. Tanaka, D.M. Williams, P. Gros, J. Pelletier, T.R. Parr, A.R. Far, A new class of small molecule RNA polymerase inhibitors with activity against rifampicin-resistant *Staphylococcus aureus*, *Bioorg. Med. Chem.* 14 (2006) 5812–5832.
- [26] H. Hartmann, J. Liebscher, A simple method for the synthesis of 5-aryl-3-amino-2-alkoxycarbonylthiophenes, *Synthesis* (1984) 275–276.
- [27] F. Fabis, S. Jolivet-Fouchet, M. Robba, H. Landelle, S. Rault, Thiatsatoic anhydrides: efficient synthesis under microwave heating conditions and study of their reactivity, *Tetrahedron* 54 (1998) 10789–10800.
- [28] L. Foulon, E. Braud, F. Fabis, J.C. Lancelot, S. Rault, Synthesis and combinatorial approach of the reactivity of 6- and 7-arylthieno [3,2-*d*][1,3] oxazine-2,4-diones, *Tetrahedron* 59 (2003) 10051–10057.
- [29] F.X. Le Foulon, E. Braud, F. Fabis, J.C. Lancelot, S. Rault, Solution-phase parallel synthesis of a 1140-member ureidothiophene carboxylic acid library, *J. Comb. Chem.* 7 (2005) 253–257.
- [30] J.G. Topliss, Utilization of operational schemes for analog synthesis in drug design, *J. Med. Chem.* 15 (1972) 1006–1011.
- [31] Molecular Operating Environment (MOE), 2011.10, Chemical Computing Group Inc., 1010 Sherbooke St. West, Suite #910, Montreal, QC, Canada, H3A 2R7, 2011.
- [32] H. Nikaido, Molecular basis of bacterial outer membrane permeability revisited, *Microbiol. Mol. Biol. Rev.* 67 (2003) 593–656.
- [33] C.M. Morris, A. George, W.W. Wilson, F.R. Champlin, Effect of polymyxin B nonapeptide on daptomycin permeability and cell surface properties in *Pseudomonas aeruginosa*, *Escherichia coli*, and *Pasteurella multocida*, *J. Antibiot.* 48 (1995) 67–72.
- [34] H. Nikaido, Outer membrane of *Salmonella typhimurium*. Transmembrane diffusion of some hydrophobic substances, *Biochim. Biophys. Acta* 433 (1976) 118–132.
- [35] A. Srivastava, D. Degen, Y.W. Ebricht, R.H. Ebricht, Frequency, spectrum, and fitness costs of resistance to myxopyronin in *Staphylococcus aureus*: myxopyronin resistance has non-zero fitness cost, *Antimicrob. Agents Chemother.* 56 (2012) 6250–6255.
- [36] S. Cabani, P. Gianni, V. Mollica, L. Lepori, Group contributions to the thermodynamic properties of non-ionic organic solutes in dilute aqueous solution, *J. Sol. Chem.* 10 (1981) 563–595.
- [37] E. Freire, Do enthalpy and entropy distinguish first in class from best in class? *Drug Discov. Today* 13 (2008) 869–874.
- [38] J. Hauptenthal, K. Hüsecken, M. Negri, C.K. Maurer, R.W. Hartmann, Influence of DNA template choice on transcription and inhibition of *E. coli* RNA polymerase, *Antimicrob. Agents Chemother.* 56 (2012) 4536–4539.
- [39] H.B. Schlegel, G.E. Scuseria, M.A. Robb, J.R. Cheeseman, Gaussian 03, Revision c.02, Gaussian Inc., Wallingford CT, 2004.
- [40] Compound **23** was synthesized via the following route:

